Cu nuclear quadrupole resonance and far-infrared reflectance of superconducting $(Y_{1-y}Ca_y)Ba_2Cu_3O_6$

A. J. Vega, M. K. Crawford, E. M. McCarron, and W. E. Farneth
Central Research and Development Department, E. I. du Pont de Nemours and Company, Experimental Station, P.O. Box 80356, Wilmington, Delaware 19880-0356
(Received 24 April 1989)

^{63}Cu and ^{65}Cu nuclear-quadrupole-resonance spectra of a series of materials of composition $(Y_{1-y}Ca_y)Ba_2Cu_3O_{6+\delta}$ with $0<y<0.5$ and $\delta \ll 1$ are reported. For $y>0.1$ these materials are superconducting with T_c around 45 K. For y values below 0.25 the spectra consist of two components. One signal is identical to that of Cu(1) in $YBa_2Cu_3O_6$, showing that the chain sites are not affected by the hole doping that accompanies substitution of Ca for Y. The other signal, which can be assigned to Cu(2) sites, is identical for all superconducting samples in the series and is not observed when $y<0.1$. Relaxation times indicate that the Cu(1) nuclei are in insulating environments, while the Cu(2) sites are conducting. Thus the conductivity is highly anisotropic. This is also demonstrated by far-infrared reflectance spectra. As Ca is added to $YBa_2Cu_3O_6$, there is a gradual decrease in the strength of the E_u (*ab* plane) modes due to free-carrier screening. The A_{2u} (*c*-axis) modes, on the other hand, remain unscreened at low frequencies.

I. INTRODUCTION

We have recently reported the discovery of superconductivity ($T_c \sim 50$ K) in a material of composition $(Y_{0.8}Ca_{0.2})Ba_2Cu_3O_{6.1}$, where the Ca atoms occupy Y sites.[1] This composition is, in fact, one member of a series of materials, $(Y_{1-y}Ca_y)Ba_2Cu_3O_{6+\delta}$ where $0 \le y \le 0.25$. This series can be thought of as parallel to the familiar $YBa_2Cu_3O_x$ series with oxidation of the Cu-O framework accomplished by metal ion substitution rather than oxygen intercalation.[2] As in the oxygen stoichiometry series, the Ca-doped material transforms from an antiferromagnetic insulator to a metallic superconductor as y is increased. In this paper we report results of Cu nuclear-quadrupole-resonance (NQR) and far-infrared (FIR) reflectance measurements which characterize this progression. As y goes from 0 to 0.25, one new NQR signal due to the metallic Cu sites in the CuO_2 sheets develops. The simplicity of the Ca series contrasts with the oxygen stoichiometry series where a number of new NQR signals resulting from changes in Cu coordination environments accompany the electronic structure changes.[3-10] The FIR spectra of the calcium series trace the development of a free-carrier plasma which is more anisotropic than in $YBa_2Cu_3O_7$. We believe that $(Y_{1-y}Ca_y)Ba_2Cu_3O_6$ will be an excellent system for coupling experimental and theoretical approaches toward understanding the electronic structure of layered cuprates. It should be noted that the Ca substitution in $YBa_2Cu_3O_x$ has been reported previously,[11] but not specifically in the O_6 structure.

II. EXPERIMENTAL

Samples of $(Y_{1-y}Ca_y)Ba_2Cu_3O_{6+\delta}$ were prepared from the binary oxides by first forming oxidized materials in air at 950 °C following the method of Manthiram *et al.*[11] and subsequently reducing them in flowing Ar at 725 °C. X-ray powder patterns for the compositions $0 \le y \le 0.25$ imply nearly single phase tetragonal material having structures analogous to $YBa_2Cu_3O_6$. Small amounts of $BaCuO_2$ are observed at $y=0.25$, and the fraction of this and other impurity phases grows for higher nominal Ca contents. The paramagnetic susceptibility at 25 °C increases with nominal Ca concentration for $y=0.0 \rightarrow 0.50$. This probably reflects an increasing paramagnetic impurity content (perhaps $BaCuO_2$) with bulk Ca content.

We have previously reported neutron-diffraction data on one of these compositions.[1] Both the neutron refinements and vacuum thermogravimetric analysis (TGA) suggest that $\delta \le 0.2$ after the Ar anneal. Vacuum reduction can be used to remove the residual oxygen to give the limiting O_6 stoichiometry without qualitatively changing material properties (as we will show). Superconductivity is observed in these tetragonal structures for $0.1 \le y \le 0.5$. Results of magnetic-flux exclusion measured by ac inductance are shown in Fig. 1.[12] The onset of flux exclusion occurs at the same temperature (~ 50 K) for all members of the series. However, the size of the effect varies with the nominal Ca content and reaches a maximum around $y=0.25$. This indicates that the nature of the superconducting phase is essentially identical for each level of Ca substitution, but that its volume fraction varies. Transmission electron microscopy indicates that there can be extended regions of pure $YBa_2Cu_3O_6$ in the low Ca preparations. We believe that beyond the nominal $y=0.25$ concentration, the superconducting volume diminishes due to the formation of impurity phases.

Details of the NQR data collection procedure have been described previously.[3] Briefly, room-temperature

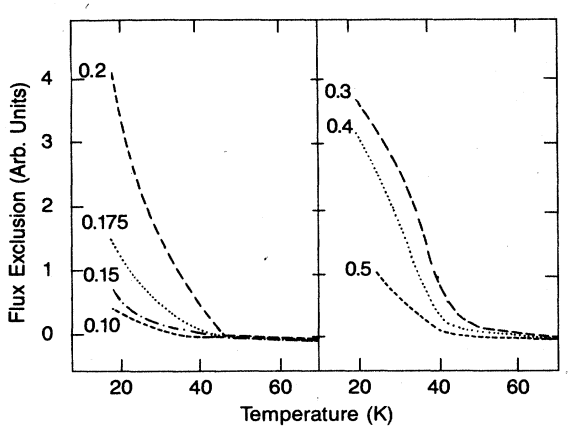

FIG. 1. Magnetic flux exclusion measurements for $(Y_{1-y}Ca_y)Ba_2Cu_3O_{6+\delta}$ with $0.1 \leq y \leq 0.5$.

NQR line shapes were determined point by point using a two-pulse echo sequence with a pulse separation of 20 μsec. Absolute signal intensities were determined which allowed Cu spin counting with an accuracy of $\pm 15\%$. Far-infrared reflectance methods have also been described previously.[13] After data collection, ~ 1000 Å of Al was deposited on the pellet surface and the reflectance measured again. This information was then used to correct the spectrum for effects due to geometric scattering.

III. RESULTS

A. NQR

NQR spectra of samples with $y = 0-0.5$ are shown in Fig. 2. Figure 3 shows the effect of additional sample reduction on the NQR spectrum of the $y = 0.15$ sample. In these figures the NQR intensity at each frequency has been divided into long-T_1 (> 10 msec) and short-T_1 (< 1 msec) components which were measured by choosing the appropriate delay time following saturation. T_1 and T_2 relaxation time measurements are summarized in Table I. We associate the long-T_1 signal components with Cu atoms in nonconducting environments and the short-T_1 components with Cu atoms in conducting environments.[3]

All the spectra in Figs. 2 and 3 are combinations of one or more of the following three signal components:

(1) A long-T_1 signal pair at 29.9 and 27.6 MHz (for ^{63}Cu and ^{65}Cu, respectively). This is the same signal as that of Cu(1) in $YBa_2Cu_3O_6$, i.e., the twofold coordinated Cu atoms in the (oxygen-vacant) chains.[3-6]

(2) A broad short-T_1 signal that extends from 22 to 29 MHz. This signal has the same profile for all the samples of this series in which it appears. The intensity of this signal is a measure of the number of Cu atoms that participate in the conduction process. The spectra indicate that metallic conductivity sets in at a y value between 0.05 and 0.10. The number of Cu atoms participating in the conduction process is roughly constant from $y = 0.15$ to the Ca solubility limit (see below).

(3) A long-T_1 signal pair at 31.2 and 28.8 MHz. This signal is only observed in the $y = 0.5$ sample.

We will first concentrate on the spectra for $y \leq 0.25$. These spectra are remarkably simple in that only two signals are observed, one clearly arising from the Cu(1) sites (the 29.9, 27.6 MHz pair), and the other (the broad 22–29 MHz signal) from the Cu(2) sites in the CuO_2 sheets. The $y = 0.5$ spectrum is somewhat more complex and is discussed separately.

The Cu(1) signals and their T_1's indicate that these Cu sites do not participate in the conduction process, in contrast to their role in $YBa_2Cu_3O_7$.[3] In superconducting $YBa_2Cu_3O_7$, T_1's of both the Cu(1) and Cu(2) nuclei are < 0.3 msec. These short relaxation times indicate that bands associated not only with Cu(2) but also with Cu(1) are partially filled and therefore conducting. In superconducting $(Y,Ca)Ba_2Cu_3O_6$ the T_1 of the Cu(1) nucleus remains > 100 msec, indicating that in these compositions, the Cu(1) sites are not involved in the conduction process. The NQR frequencies of the Cu(1) peaks coincide exactly with those of the parent compound $YBa_2Cu_3O_6$ for all Ca contents. The Cu(1) atoms, therefore, do not undergo significant structural change when Ca is substituted for Y. This is consistent with neutron structural data.[1] There is, however, a gradual broaden-

TABLE I. NQR relaxation times T_1 and T_2 measured at specific frequencies in $(Y_{1-y}Ca_y)Ba_2Cu_3O_{6+\delta}$.

	T_1 (msec) at			T_2 (μsec)[a] at		
y	25 MHz	29.9 MHz	31.2 MHz	25 MHz	29.9 MHz	31.2 MHz
0.00		190			180	
0.05		60				
0.10		110				
0.15		140				
0.15 (red)[b]	0.12	120		38	600	
0.20		140				
0.25		120		42	370(G)	
0.5	0.3	120	18		450(G)	260(G)

[a] T_2 values designated by (G) represent a Gaussian decay, $\exp[-(t/T_2)^2]$.
[b] Sample reduced in vacuum.

ing of the peaks, which implies small variations in the local structure at Cu(1).

In $YBa_2Cu_3O_6$ the Cu(2) signal cannot be observed in the frequency range that we have studied because the antiferromagnetically ordered electron spins in the CuO_2 layers create strong internal magnetic fields.[5] However, when the Ca content is 0.10 or larger, Cu(2) sites are detected as a short-T_1 signal. The electron holes introduced by Ca substitution induce a delocalization of the ordered electron spins, allowing conduction to occur. The corresponding Cu(2) NQR signals appear in the 20–30 MHz frequency range. The NQR line shape of the conducting Cu atoms shown in Figs. 2 and 3 is a combination of ^{63}Cu and ^{65}Cu signals. The ^{63}Cu components were estimated by a numerical deconvolution procedure[3] and the results for $y = 0.15$ and 0.25 are shown in Fig. 4, together with examples of the conducting ^{63}Cu signal of oxygen-doped $YBa_2Cu_3O_x$ in each of the two T_c plateaus of 90 K ($7.0 > x > 6.9$) and 55 K ($6.8 > x > 6.4$).[3,14] The line shapes of the Ca-doped samples are almost identical, but they differ significantly from either of the $YBa_2Cu_3O_x$ signals. These three materials have the same basic lattice structure. NQR demonstrates that the electric charge distributions in the vicinity of the Cu(2) sites are quite different, however. While this may partly be related to variations in bond lengths, the frequency shifts are most likely dominated by differences in the hybridization and occupancy of the electronic wave functions.[10] The T_2 relaxation times of the signals in the Ca-doped superconductor are about 40 μsec, which is also significantly shorter than the values of around 90 μsec which we have measured for the conducting Cu atoms in $YBa_2Cu_3O_x$.[3]

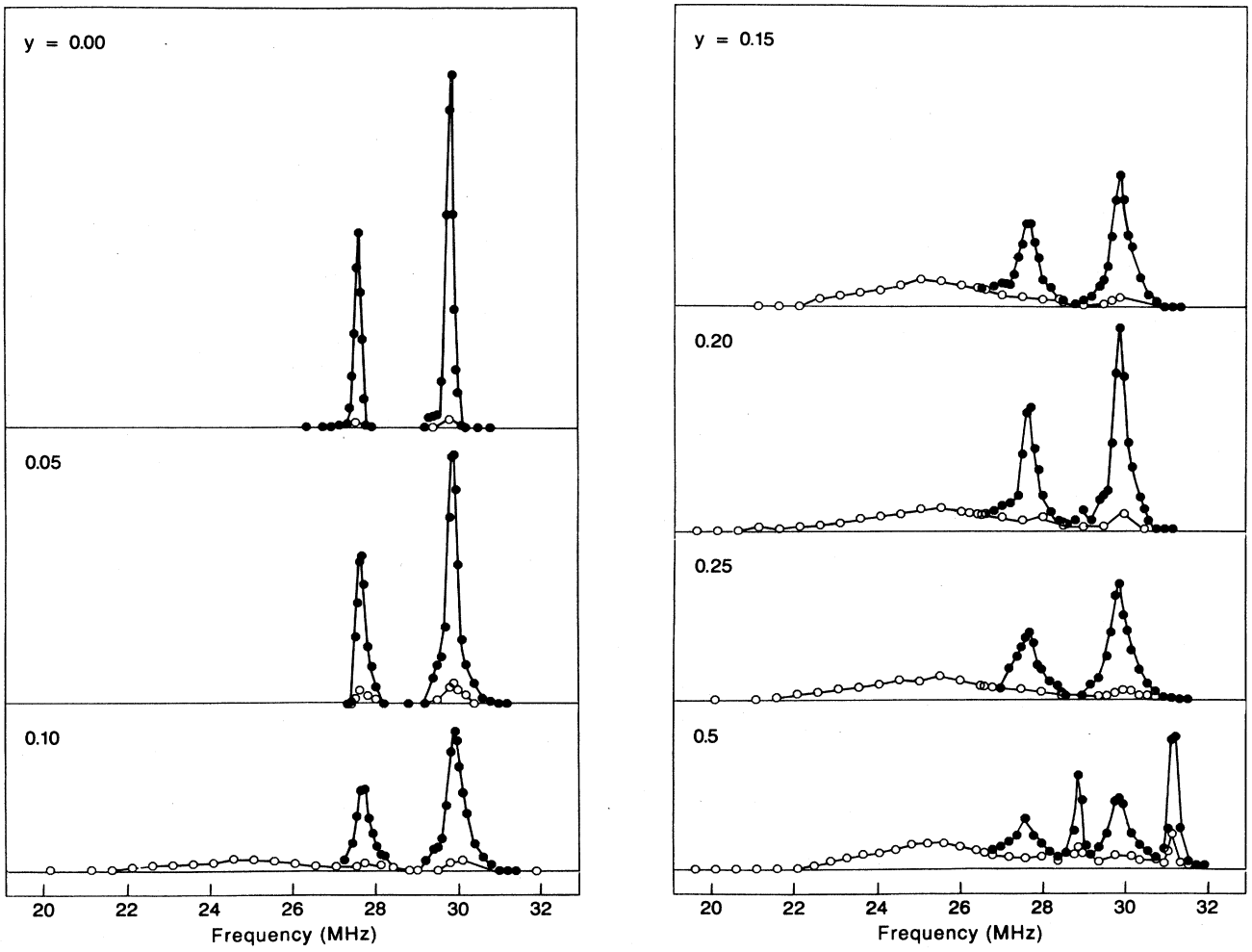

FIG. 2. Room-temperature Cu NQR spectra of $(Y_{1-y}Ca_y)Ba_2Cu_3O_{6+\delta}$ with y values as indicated. The signal intensities are normalized to Cu weight, divided by the square of the frequency, and plotted on a uniform intensity scale. The signals are not corrected for echo intensity reductions due to T_2. The open and solid symbols represent components with $T_1 < 1$ and > 10 msec, respectively.

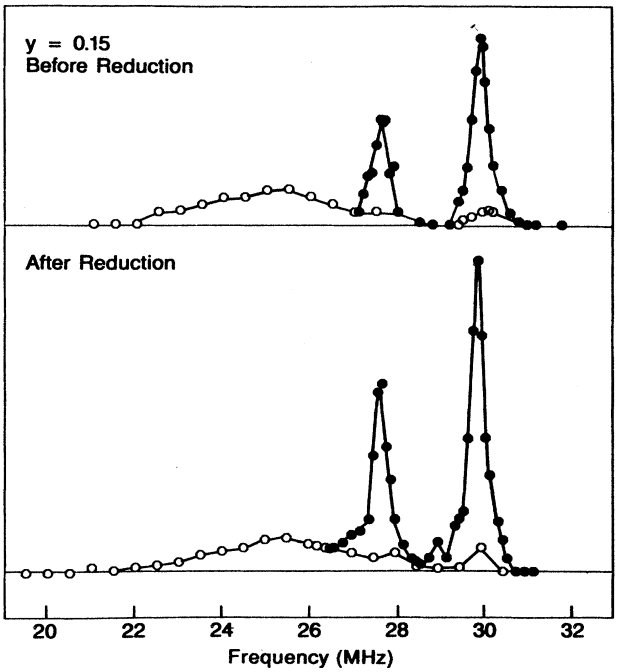

FIG. 3. Room-temperature Cu NQR spectra of $(Y_{0.85}Ca_{0.15})Ba_2Cu_3O_{6+\delta}$ before and after sample reduction in vacuum. Symbols and relative intensities as in Fig. 2.

Integrated intensities of the Cu(1) and Cu(2) signals are listed in Table II. All data have been corrected for T_2 relaxation. If the samples were microscopically homogeneous, then one would expect integrated intensities of 1 and 2 for the long-T_1 Cu(1) and short-T_1 Cu(2) signals, respectively. These intensities, however, depend on sample preparation variables. In the Ar annealed samples, the number of Cu(1) sites that contribute to the spectrum is generally smaller than 1. The low Cu(1) intensities are probably the result of residual oxygen in the chain sites. An oxygen stoichiometry of $O_{6.1}$ has been determined by TGA and neutron diffraction for this material. Indeed, in the sample that has been further reduced by heating in

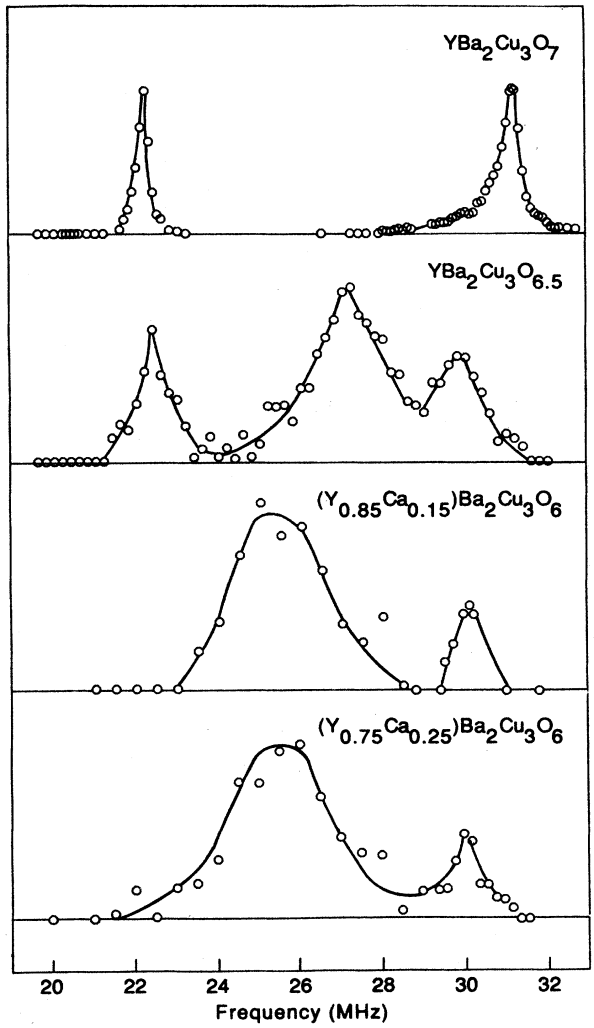

FIG. 4. Short-T_1 ^{63}Cu components of the Cu NQR spectra of $YBa_2Cu_3O_{7.0}$ (T_c=88 K), $YBa_2Cu_3O_{5.1}$ (T_c=57 K), $(Y_{0.85}Ca_{0.15})Ba_2Cu_3O_{6+\delta}$ (T_c=50 K), and $(Y_{0.75}Ca_{0.25})Ba_2Cu_3O_{6+\delta}$ (T_c=50 K). The plotted data points were obtained by a numerical deconvolution of the short-T_1 components of spectra presented in Ref. 3 and in Fig. 2.

TABLE II. Integrated intensities of NQR signal components of $(Y_{1-y}Ca_y)Ba_2Cu_3O_{6+\delta}$, corrected for T_2 relaxation decay, converted to numbers of Cu atoms per formula unit.

	Signal component with ^{63}Cu frequency:		
y	below 29 MHz	at 29.9 MHz	at 31.2 MHz
0.00	0.0	0.8	0.0
0.05	<0.04	0.9	0.0
0.10	0.9	0.7	0.0
0.15	1.2	0.6	0.0
0.15 (red)[a]	1.2	1.0	0.0
0.20	1.3	0.7	0.0
0.25	1.4	0.5	0.0
0.5	1.3	0.6	0.3

[a]Sample reduced in vacuum.

vacuum, the Cu(1) signal sharpens and approaches the expected integrated intensity of 1.0 (Fig. 3, Table II). This clearly demonstrates that *all* the Cu(1) sites preserve their geometric and electronic characteristics as the crystal is doped with Ca, not just those that may be close to undoped Y sites. At the same time, Fig. 3 shows that the Cu(2) signal is not affected by the removal of residual oxygen. For all samples with y between 0.15 and 0.5, the integrated intensity of the conducting component of the spectrum corresponds to only about 60–70% of the Cu(2) atoms. The remaining Cu(2) sites must have structural or electronic properties that prevent their NQR detection under the present experimental conditions. Ca substitution may not be microscopically homogeneous.[15] This would leave some Cu(2) atoms unobservable due to local antiferromagnetic ordering. Some inhomogeneity is also suggested by the superconducting volume fraction changes evident in the flux exclusion data shown in Fig. 1.

The sample with $y=0.5$ shows an additional pair of long-T_1 peaks for which the ^{63}Cu signal is at 31.2 MHz. An NQR peak at this frequency has now been observed in several samples in the 1:2:3 family, but with widely varying relaxation behavior. The signal is observed in $YBa_2Cu_3O_x$ having $T_c \sim 90$ K ($6.9 < x < 7.0$). In those samples the room-temperature T_1 is less than 0.3 msec. The signal then clearly represents the conducting Cu(2) sites.[3,16] In $YBa_2Cu_3O_x$, with $T_c \sim 55$K ($6.4 < x < 6.8$), an NQR peak is observed at the same frequency, but with a T_1 of the order of 100 msec.[3,10] This signal may be assigned to either two-coordinated monovalent Cu(1) sites[10] or to Cu(2) atoms with a d-electron configuration that is similar to that of $YBa_2Cu_3O_7$.[3] Whatever the specific assignment may be, the long-T_1 signal at 31.2 MHz appears to arise from a particular structural component of the 1:2:3 samples. Therefore, it is unlikely that the 31.2-MHz peak in Fig. 2 results from Cu atoms in the impurity phases found in $(Ca_{0.5}Y_{0.5})Ba_2Cu_3O_6$ sample preparations.[1] In fact, we have verified that $BaCuO_2$, which appears to be a major impurity, does not give an NQR signal at 31.2 MHz.

B. Far-infrared reflectance

Far-infrared reflectance (FIR) measurements also yield information concerning the effects of Ca^{2+} for Y^{3+} substitution on the electronic structure of $(Y,Ca)Ba_2Cu_3O_6$. The FIR spectrum changes dramatically with increasing Ca content in a way that is consistent with increasing metallic character (Fig. 5). The phonon response is screened by the free-carrier plasma, leading to a decreased TO-LO splitting and the eventual disappearance of the phonons from the FIR spectrum. Furthermore, the *ab* plane modes are specifically screened, implying that the conductivity is essentially two dimensional.

Assignments of the phonons in $YBa_2Cu_3O_6$ based on both ceramic and single-crystal data have been given.[17] There are eleven infrared active phonons ($5A_{2u}+6E_u$). Of these, the A_{2u} phonons are c-axis polarized, whereas the E_u phonons are polarized in the *ab* plane. As Ca is added to $YBa_2Cu_3O_6$, there is a gradual decrease in the strength of the E_u modes due to the effective free-carrier screening in the *ab* plane. This effect can be clearly observed in Fig. 5 (see, for example, modes at 188 and 250 cm^{-1}). It was also evident in the series $YBa_2Cu_3O_x$

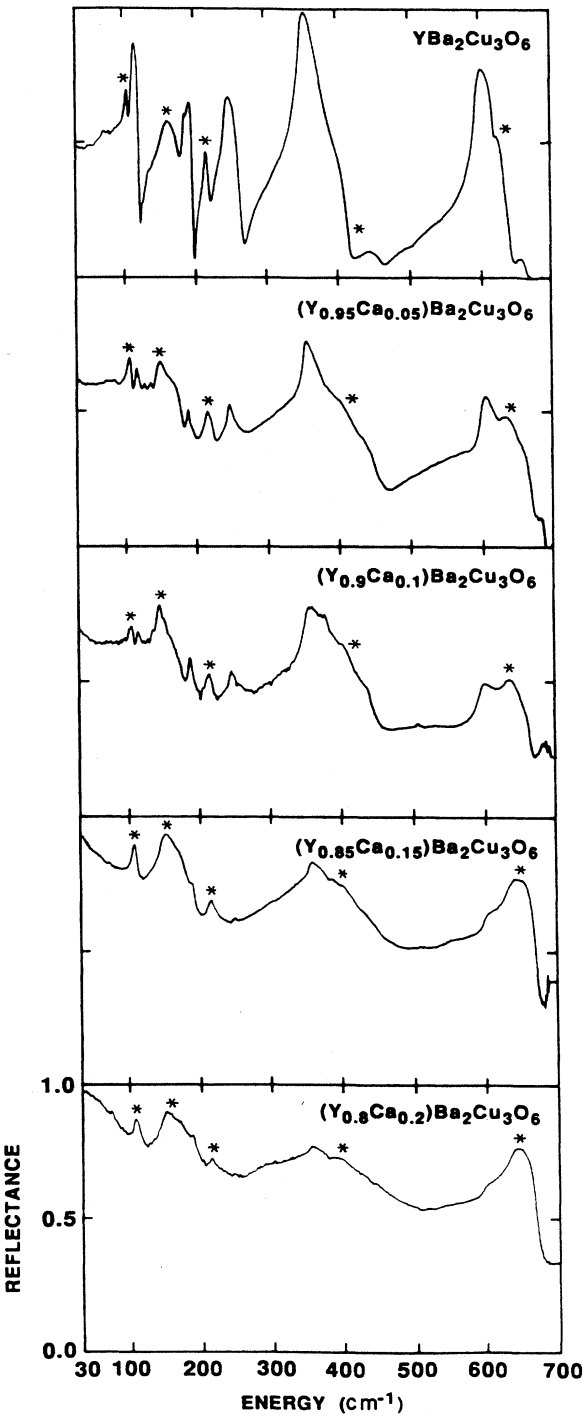

FIG. 5. Far-infrared reflectance spectra from 30–700 cm^{-1} of $(YCa)Ba_2Cu_3O_6$ at 10 K. Asterisks mark the A_{2u} c-axis modes.

where doping was accomplished by oxygen stoichiometry changes.[13] The A_{2u} modes, however, are clearly visible throughout the sequence. Of particular interest is the phonon of A_{2u} symmetry at 108 cm^{-1}, which has been assigned to a c-axis Ba vibration.[17] In $YBa_2Cu_3O_x$ the 108-cm^{-1} Ba vibration is only observed for $x \leq 6.6$. When $x > 6.6$, the development of a low-frequency (≤ 200 cm^{-1}) c-axis plasma response can be inferred from the complete screening of the 108-cm^{-1} Ba vibration and the more gradual changes in the 150- and 190-cm^{-1} phonons. The smaller the TO-LO splitting for a given mode, the more easily it is screened by a plasma response and therefore the Ba A_{2u} mode, which has a TO-LO splitting[17] of only 2 cm^{-1}, is a particularly sensitive probe of the conductivity along the c axis. In $(Y_{1-y}Ca_y)Ba_2Cu_3O_6$, the very low conductivity along the c axis allows observation of the 108-cm^{-1} Ba A_{2u} mode throughout the entire doping range. Another interesting comparison between the oxygen- and Ca-doped series involves the 650-cm^{-1} A_{2u} mode, which is a Cu(1)-O c-axis asymmetric stretching vibration.[13,17] This mode does not change in frequency with Ca doping. This implies little, if any, change in the Cu(1)-O(4) bonding as a result of Ca doping. In contrast, this mode has shifted to 570 cm^{-1} in $YBa_2Cu_3O_7$.

IV. DISCUSSION

Our spectroscopic observations appear to be in good agreement with the picture of the electronic structure of $YBa_2Cu_3O_x$ that emerges from recent tight-binding structure calculations.[18] At $x=6$, the model assumes that all Cu(2) are at an oxidation level of Cu^{II} and all Cu(1) are effectively Cu^{I}. There is no electronic interaction between Cu(1) and Cu(2) sites. This leads to a band structure dominated by a half-filled band of Cu(2) $d_{x^2-y^2}$ character at the Fermi energy and antiferromagnetic ordering. As x increases, the doped holes can be thought of as oxidizing Cu(1) sites from Cu^{I} to Cu^{III} and simultaneously changing the local bonding arrangements in a way that drops the energy of the Cu(1) $d_{z^2-y^2}$ band. At the stoichiometry where this band drops below the Fermi energy, approximately $x=0.4$, electron transfer between Cu(1) and Cu(2) sites becomes possible. Metal character begins to emerge, because the Cu(2) sites can now be oxidized by additional filling of the O(1) sites. It is important to recognize that filling vacancies at O(1) causes local bonding changes between Cu(1) and its other coordinated oxygens, i.e., the axial oxygens O(4), and that these changes control whether the key bands in the planes and chains interact. The low-frequency c-axis plasma response that is observed in $YBa_2Cu_3O_x$ for $x \geq 0.5$ also develops as a result of the increased chain-plane band overlap. In the Ca-doped system there are no similar indirect changes in the band structure because the Cu(1)-O bonding is not altered as the system is oxidized. Therefore, the half-filled Cu(2) $d_{x^2-y^2}$ bands at the Fermi energy are oxidized directly by the substitution of Ca for Y, and metal character is restricted to the Cu(2) planes. This certainly appears to be the case as we have documented with our NQR and FIR experiments—the Cu(1) sites remain insulating, and a low-frequency c-axis plasma does not develop.

V. CONCLUSIONS

In summary, the progressive substitution of Ca for Y in $(Y_{1-y}Ca_y)Ba_2Cu_3O_6$ leads to a series of materials that cross the boundary from insulating/antiferromagnetic to metallic/superconducting. Cu NQR and FIR reflectance spectra paint a very simple picture for the changes in the normal-state electronic structure that accompany this progression. For Ca substitution up to $y=0.25$, Cu(1) sites are unaffected. Holes generated in the Ca for Y substitution go into the CuO_2 planes and induce a breakdown in the antiferromagnetic ordering. The Cu(2) sites begin to develop conducting electronic character at $y \sim 0.1$. These conducting environments occur with a range of local atomic structures and maximize in intensity at $y \sim 0.25$. The E_u phonons are screened by the ab plane free-carrier plasma, while the A_{2u} phonons are not screened. The intercalation of small amounts of oxygen in the nominally vacant chain sites has no effect on the electronic state of the CuO_2 planes. Like the recently reported $Pb_2Sr_2CaCu_3O_x$ system,[19] $(Y,Ca)Ba_2Cu_3O_6$ appears to be a highly anisotropic (two-dimensional) metal. We expect that this will be one of the most anisotropic high-temperature superconductors and, because of its relatively simple crystal structure, serve as a model two-dimensional system.

ACKNOWLEDGMENTS

We are grateful to Pratibha Gai for electron microscopy, R. Flippen for magnetic measurements, and J. Parise and H. Horowitz for helpful discussion. W. Dolinger, R. Balback, R. Smalley, and M. Sweeten provided excellent technical assistance.

[1]E. M. McCarron, M. K. Crawford, and J. B. Parise, J. Solid State Chem. **78**, 192 (1989).

[2]W. E. Farneth, R. K. Bordia, E. M. McCarron, M. K. Crawford, and R. B. Flippen, Solid State Commun. **66**, 953 (1988); and references therein.

[3]A. J. Vega, W. E. Farneth, E. M. McCarron, and R. K. Bordia, Phys. Rev. B **39**, 2322 (1989).

[4]W. W. Warren, R. E. Walstedt, R. F. Bell, G. F. Brennert, R. J. Cava, G. P. Espinosa, and J. P. Remeika, Physica C **153-155**, 79 (1988).

[5]H. Yasuoka, T. Shimizu, Y. Ueda, and K. Kosuga, J. Phys. Soc. Jpn. **57**, 2659 (1988).

[6]Y. Kitaoka, S. Hiramatsu, K. Ishida, K. Asayama, H. Takagi, H. Iwabuchi, S. Uchida, and S. Tanaka, J. Phys. Soc. Jpn. **57**, 737 (1988).

[7]L. Mihaly, I. Furo, S. Pekker, P. Banki, E. Lippmaa, V. Miidel, E. Joon, and I. Heinmaa, Physica C **153-155**, 87 (1988).

[8]H. Luetgemeier, Physica C, **153-155**, 95 (1988).

[9]Y. Kitaoka, S. Hiramatsu, Y. Kohori, K. Ishida, T. Kondo, H. Shibai, A. Asayama, H. Takagi, S. Uchida, H. Iwabuchi, and

S. Tanaka, Physica C **153-155**, 83 (1988).
[10]W. W. Warren, R. E. Walstedt, G. F. Brennert, R. J. Cava, B. Batlogg, and L. W. Rupp, Phys. Rev. B **39**, 831 (1989).
[11]A. Manthiram, S.-J. Lee, and J. B. Goodenough, J. Solid State Chem. **73**, 278 (1988); Y. Tokura, J. B. Torrance, T. C. Huang, and A. I. Nazzal, Phys. Rev. B **38**, 7156 (1988).
[12]E. M. McCarron, J. B. Parise, M. K. Crawford, and J. M. Tranquada, 1989 Industry University Advanced Materials Conference, Denver, 1989 (Advanced, Materials Institute, Golden, Colorado, in press).
[13]M. K. Crawford, W. E. Farneth, R. K. Bordia, and E. M. McCarron III, Phys. Rev. B **37**, 3371 (1988); M. K. Crawford, W. E. Farneth, E. M. McCarron III, and R. K. Bordia, *ibid.* **38**, 11 382 (1988).
[14]R. J. Cava, B. Batlogg, C. H. Chen, E. A. Rietman, S. M. Zahurak, and D. Werder, Nature **329**, 423 (1987).
[15]J. B. Parise, P. L. Gai, M. K. Crawford, and E. M. McCarron III, in *High-Temperature Superconductors,* Materials Research Society Symposium Proceedings, edited by J. B. Torrane *et al.* (Materials Research Society, Pittsburgh, Pennsylvania, in press), Vol. 156.
[16]C. H. Pennington, D. J. Durand, D. B. Zax, C. P. Slichter, J. P. Rice, and D. M. Ginsberg, Phys. Rev. B **37**, 7944 (1988).
[17]M. K. Crawford, Gerald Burns, and F. Holtzberg, Solid State Commun. **70**, 557 (1989).
[18]M.-W. Whangbo *et al.*, Inorg. Chem. **27**, 467 (1988); J. K. Burdett and G. V. Kulkarni, Phys. Rev. B (to be published).
[19]R. J. Cava *et al.*, Nature **211**, 336 (1988); M. A. Subramanian *et al.*, Physica C **157**, 124 (1989).